

Evaluation of HOM Coupler Probe Heating for 3.9 GHz cavities

G. Wu, E. Harms, T. Khabiboulline

Abstract:

The RF heating of the HOM coupler feedthrough has been evaluated for third harmonic cavities. The calculation was based on a two-leg formteil HOM coupler with shortened formteil post. The calculation of RF heating was determined by HFSS. The magnetic field seen at the feedthrough tip was at 15.6% of the cavity equator field, a rather high number. However, the overall RF heating was less dramatic at the nominal accelerating gradient 14MV/m and 0.5% duty cycle. Subsequent thermal analysis showed such RF heating will not degrade cavity performance if the JLAB-type sapphire feedthrough is used.

FNAL-TD-08-019
02/11/2008

Evaluation of HOM Coupler Probe Heating for 3.9 GHz cavities

1. Introduction

For the 3rd harmonic cavities that used two-leg formteil HOM couplers [1], the tip field was evaluated using the 3D EM solver HFSS. The JLAB-type sapphire feedthrough [2] is adopted for HOM power extraction. Thermal analysis was conducted for different situations. The result concluded the current design with sapphire feedthrough effectively eliminated potential thermal runaway phenomenon seen elsewhere [3,4]. This note describes the simulation results on the local magnetic field around the tip and its thermal effect on sapphire feedthrough.

2. RF Model

A 3D computer model was constructed as shown in Figure 1. A 3.9GHz single cell cavity is used as the resonator. A coaxial line was inserted in the opposite side beam pipe to act as an input probe to transmit RF power. The output is a 50Ω coaxial line connected to the HOM probe tip. The fillet geometries on the notch gap and the two formteil stubs inside of the HOM coupler are kept.

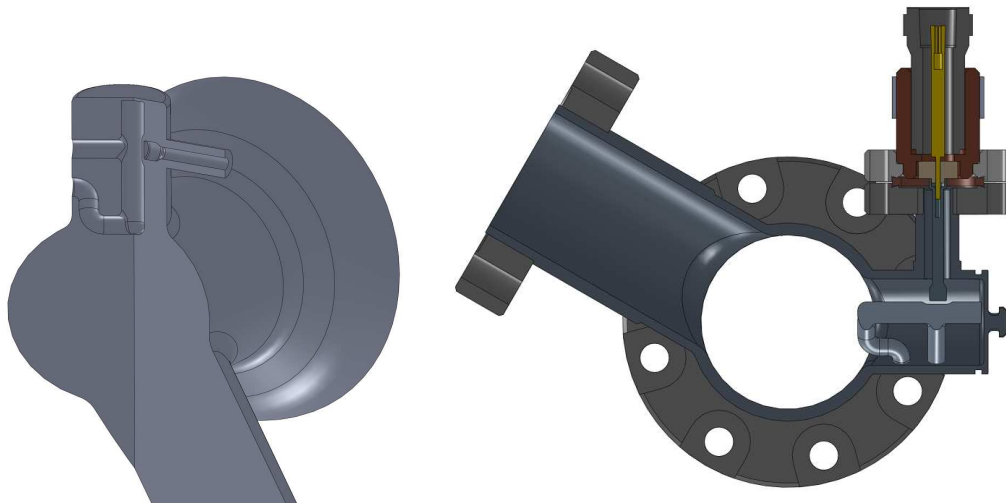


Figure 1: 3D RF model used in the HFSS™ simulation. The HOM coupler and the right side beam pipe was cut away by 135-degrees to show the inside geometry.

The computation followed procedures described elsewhere [5] to assure the proper mesh density and tuning of the notch gap. Figure 2 shows the transmission properties of the HOM coupler indicating the model is tuned to reject the fundamental mode power transmission.

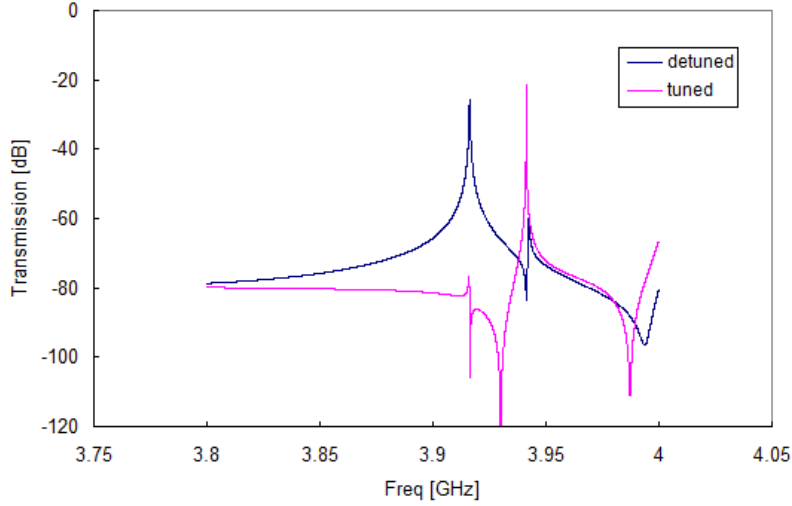


Figure 2: The frequency tuning of the notch filter.

The calculation of RF heating was made using an HFSS simulation and the measurement of the residual resistance of cavity 5. In Figure 3, the simulated magnetic field in the region around the HOM feedthrough is shown. The maximum magnetic field is found near the feedthrough probe location.

The measured residual resistance (R_s) of cavity 5 is shown in Figure 4 along with the calculated values for a typical niobium R_{res} of 50 n Ω , and a worsened niobium R_{res} of 700 n Ω . The data are consistent with $R_{res} \sim 700$ n Ω . Using the extrapolated R_{res} of 700 n Ω and the magnetic field from the simulation, the heat loss is calculated and shown in Figure 5 for a 0.5% duty cycle and 100% (CW) duty cycle. The calculated heat loss for a JLab probe (described later) operated at CW is shown for comparison.

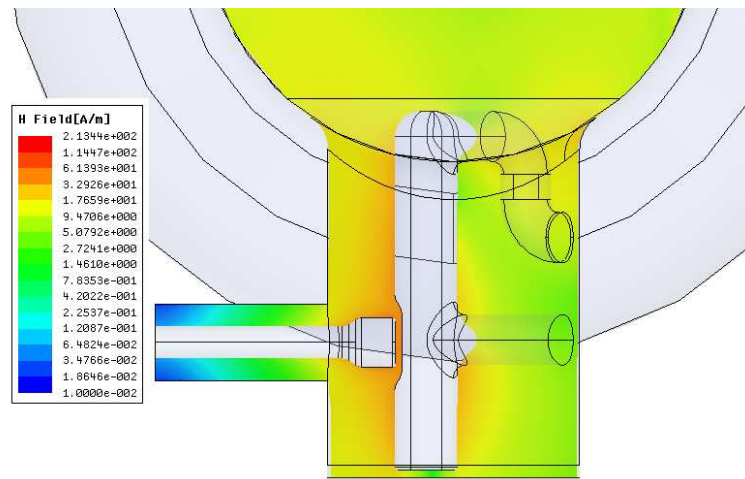


Figure 3: HFSS simulation of the magnetic field near the HOM feedthrough tip.

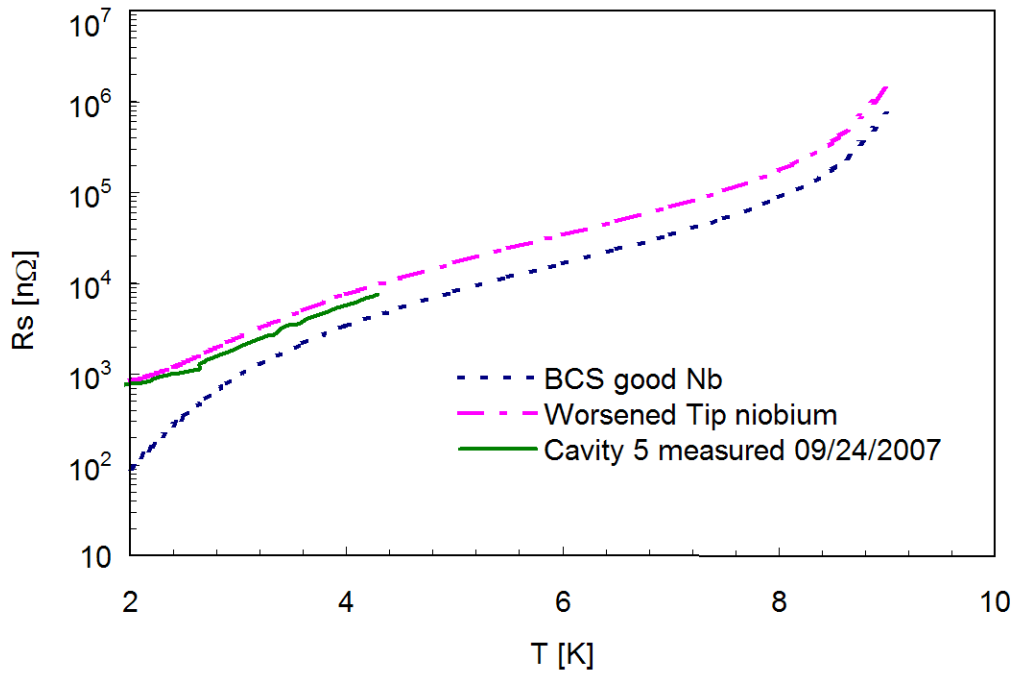


Figure 4: Surface resistance for an ideal 3.9 GHz niobium cavity; a cavity with 700 nΩ residual resistance to represent a worsened niobium tip, and the measurement of cavity 5.

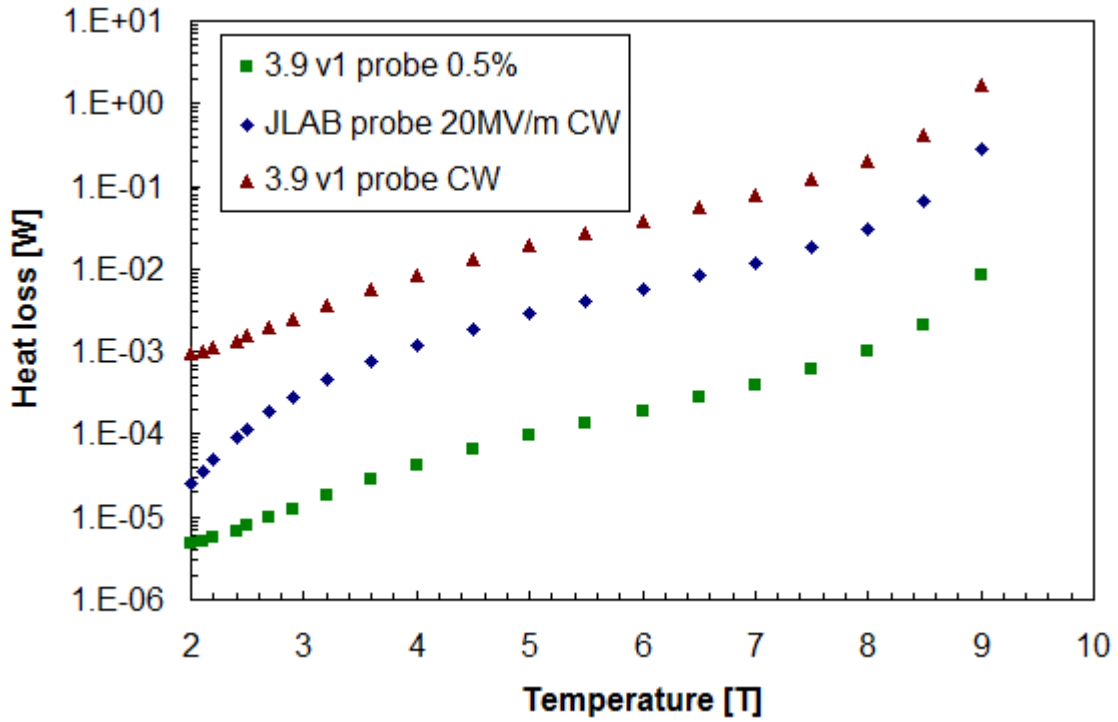


Figure 5: Tip RF heating at 0.5% operating duty cycle and CW compared to JLAB 12-GeV cavity feedthrough.

3. Thermal analysis

A detailed ANSYS model has been constructed to evaluate the effect of probe tip RF heating, cable heat loading and thermal strapping. In Figure 6 the model for entire feedthrough based on JLAB's sapphire feedthrough is shown. The full contact between the sapphire and copper sleeve was reduced to partial contact to simulate a worst case scenario for potentially inadequate brazing contact.

While the thermal conductivity (K_c) has been thoroughly and consistently characterized for oxygen-free copper, sapphire and niobium have thermal conductivity which is heavily dependent on the purity and the processing of the material. For sapphire, the thermal conductivity at 10 K can vary by an order of magnitude from vendor to vendor. In the appendix, the upper and lower bounds of K_c are plotted. The value chosen for the ANSYS simulation was between these bounds. Similarly, niobium thermal conductivity has shown large variability [6]. Based on the extended machining of the niobium tip, its thermal conductivity was extrapolated to the number equivalent to niobium with RRR around 250. The thermal effect of using different K_c for these two materials will be described later.

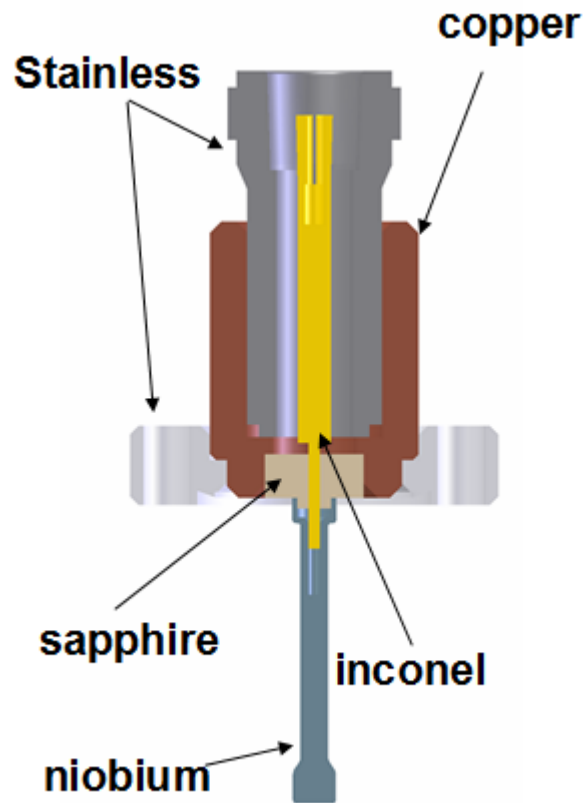


Figure 6: ANSYS model for sapphire-based feedthrough.

A thermal simulation was conducted for both vertical test and horizontal test conditions. For a vertical test, the feedthrough would be attached to a cavity and fully immersed in 2

K superfluid helium. Under certain material properties (sapphire K_c at 30% of its best value, niobium K_c at 80% of RRR 250 and BCS resistance enhanced by 1.9 of SRIMP estimation), the tip temperature remains stable up to 17 MV/m (CW). Once the cavity gradient reaches 17 MV/m, the niobium tip quickly becomes normal conducting as shown in Figure 7. The time constant to quench is 0.7 seconds with recovery time ~ 4 seconds. Data showed good agreement with experiment observation.

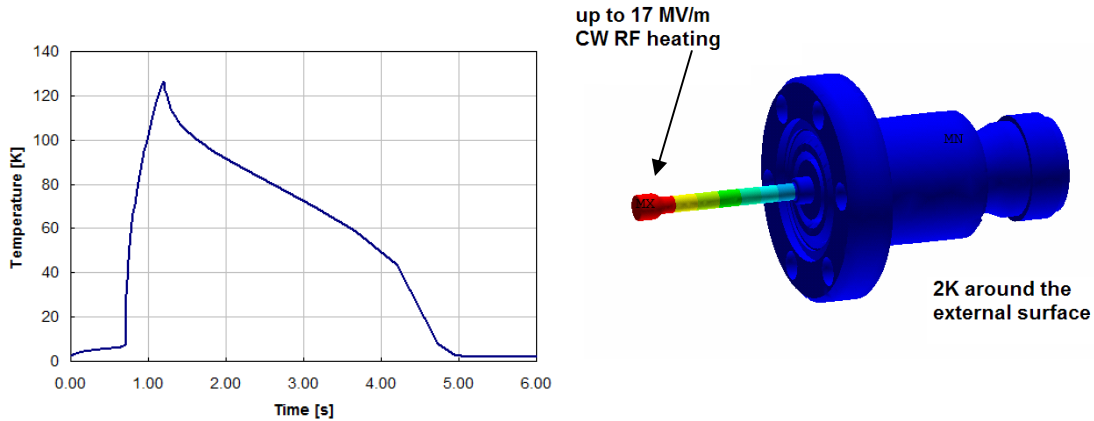


Figure 7: ANSYS thermal analysis under vertical test condition: Rising temperature at the tip end at 16 MV/m (left); Temperature profile for the tip (right).

Changing the thermal conductivity of sapphire changed the quench time slightly, as shown in Figure 8, while niobium thermal conductivity changes the tip temperature dramatically as shown in Figure 9. This is probably due to the geometrical difference between the sapphire and niobium parts of the feedthrough structure.

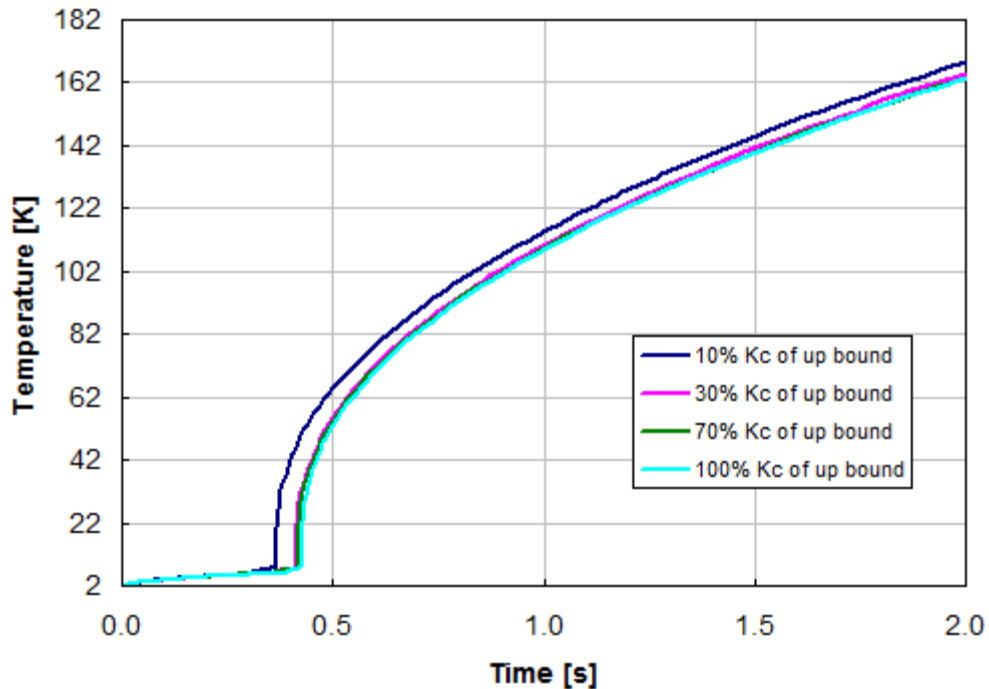


Figure 8: Niobium quench time changes slightly for different sapphire thermal conductivities.

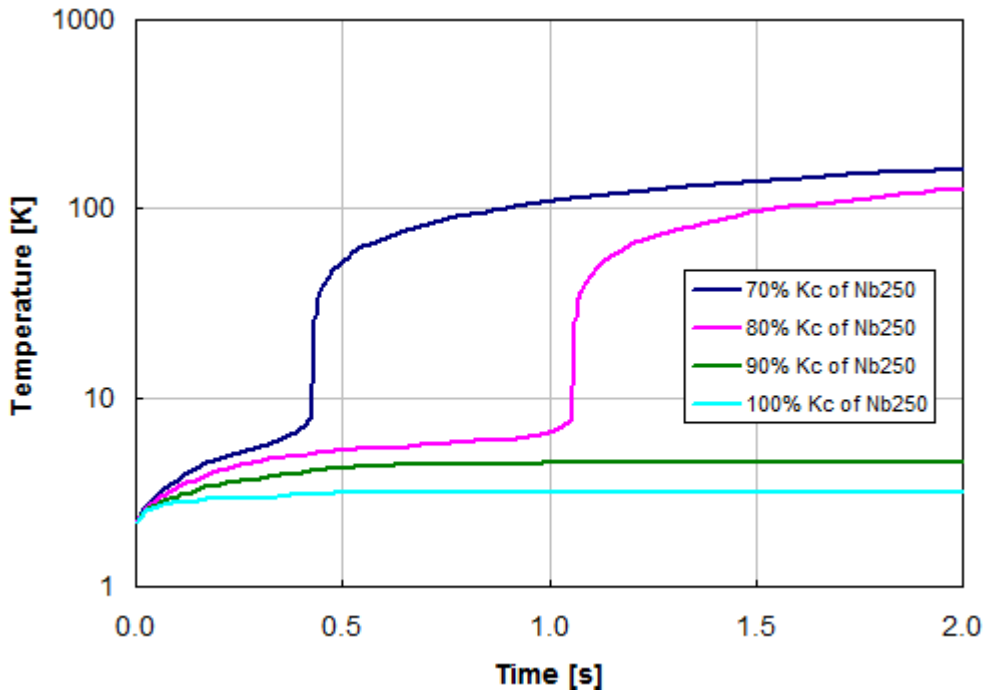


Figure 9: Niobium quench time changes dramatically for different niobium thermal conductivities.

For a fixed thermal conductivity of sapphire and niobium, the surface resistance of niobium tip can also affect the tip temperature significantly, as shown in Figure 10. The nominal BCS resistance was set at good surface quality niobium as shown in the Appendix.

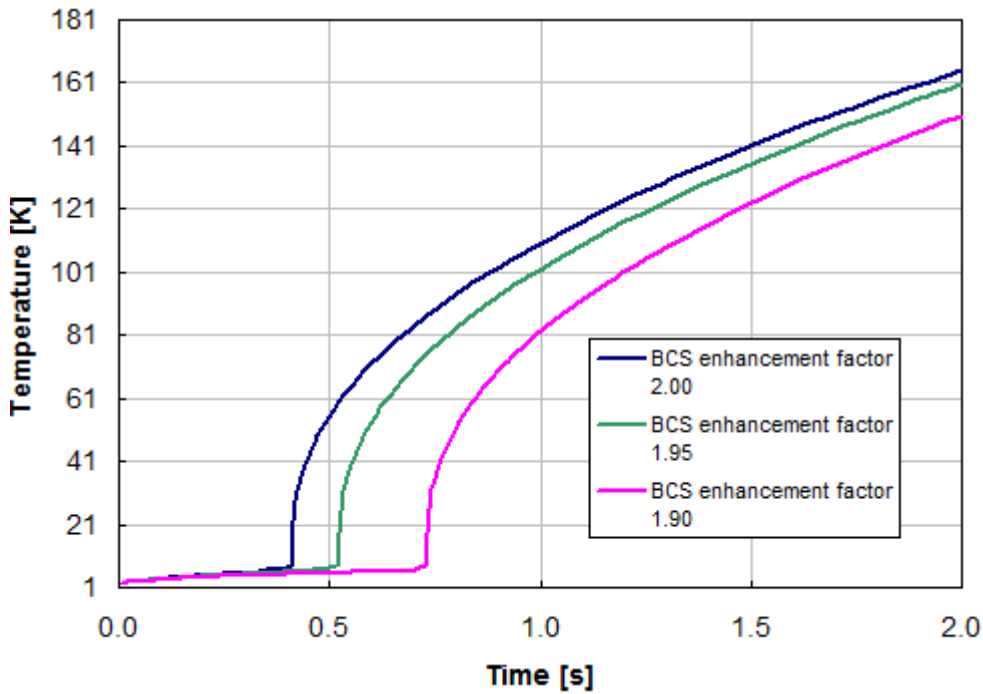


Figure 10: Niobium quench time changes dramatically for different niobium surface resistances.

If the feedthrough is attached to a cavity during a horizontal test, the RF cable constitutes a static heat load around 20 mW. If the cooling of the feedthrough tip comes only from heat conductance through the flange contact to the cavity, tip can become normal conducting and degrade the cavity performance at 14MV/m (1%) or higher. Figure 11 shows the case with the flange temperature remains at 4K and probe tip rises to 28 K.

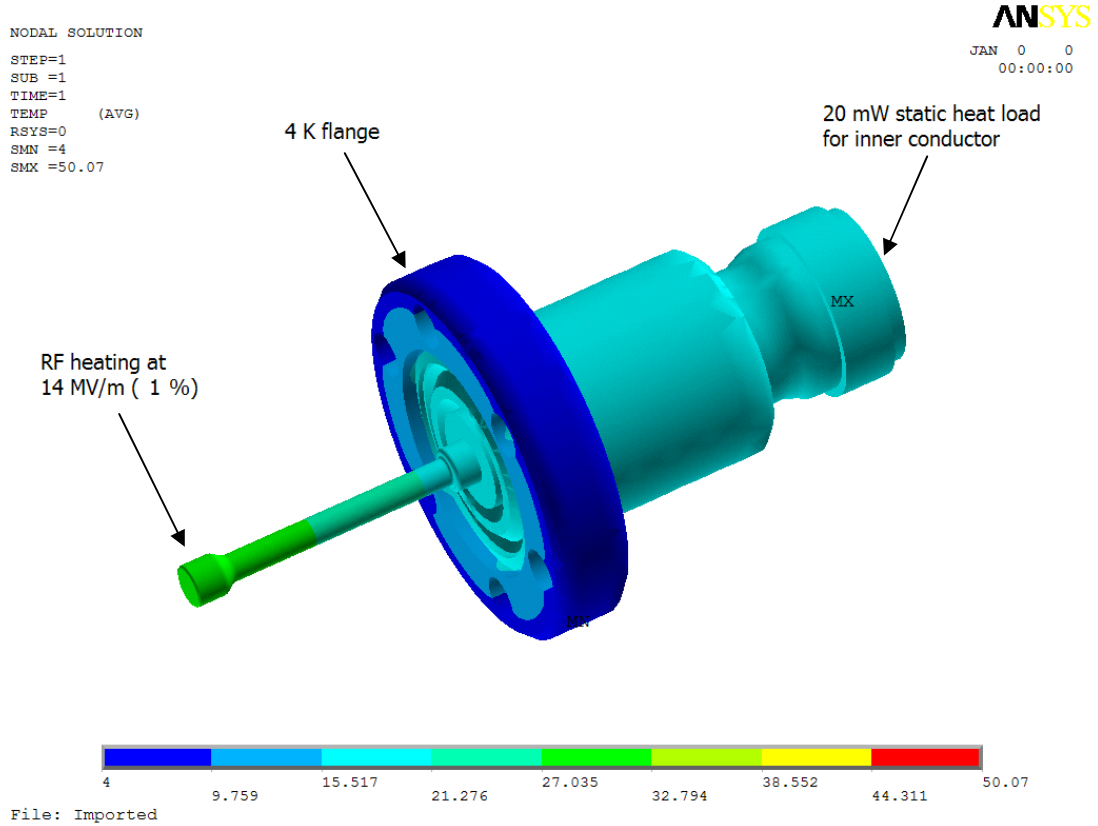


Figure 11: ANSYS thermal analysis for a horizontal test with the flange conducting the generated heat.

Once a thermal strap is added to the copper sleeve, which was the design intention of sapphire feedthrough, the probe tip temperature becomes stable, as shown in Figure 12.

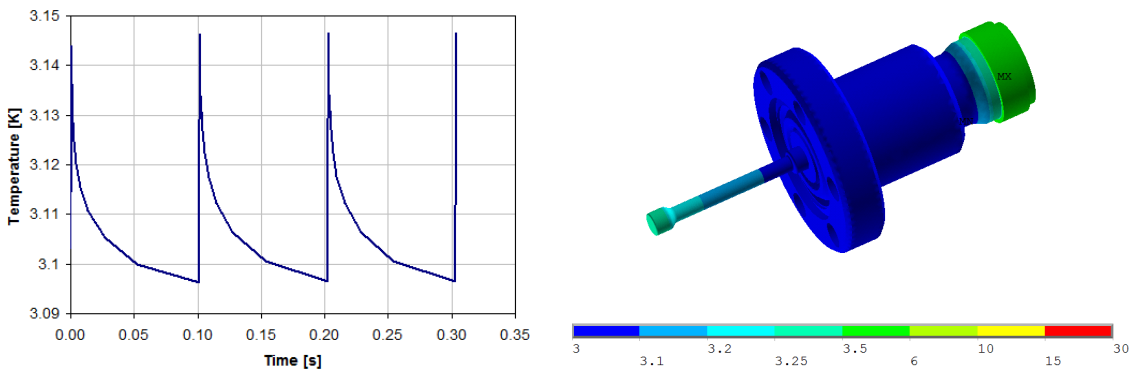


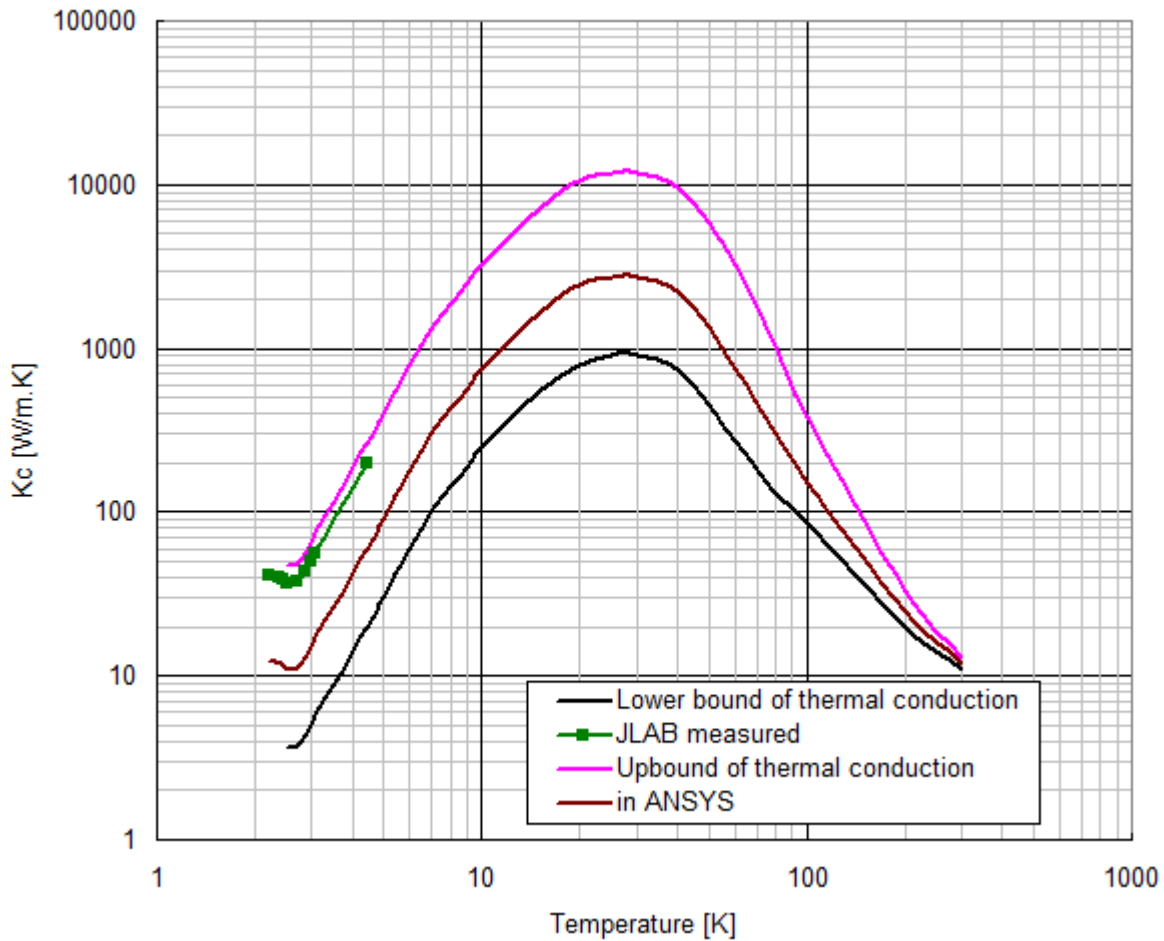
Figure 12: ANSYS thermal analysis for horizontal test conditions with thermal strap attached to the feedthrough body: Temperature pulse at the tip end (left); Temperature profile for the feedthrough (right).

When the RF power goes to CW, the feedthrough enhanced with thermal strap still manages to remain stable even at 15 MV/m, only slight below the Vertical testing performance of 17 MV/m for cavity 5.

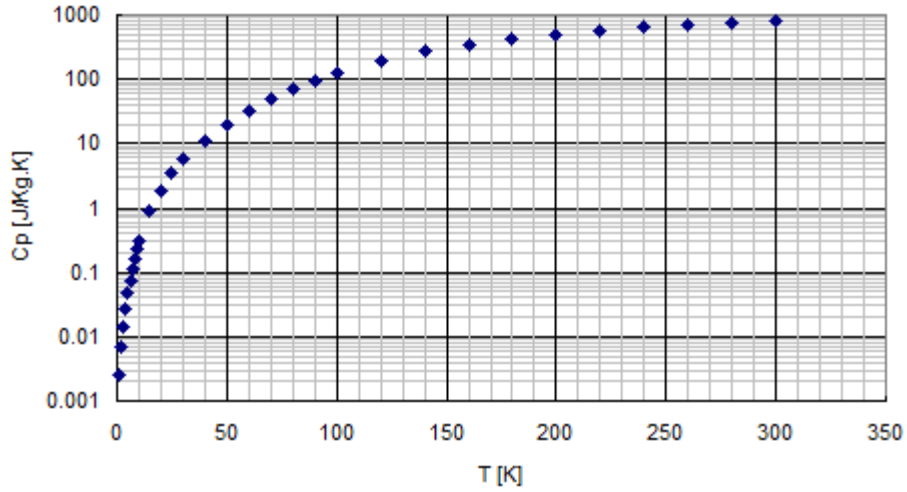
4. Acknowledgment

The authors would like to thank D. Mitchell for his modeling assistance and N. Solyak for valuable discussions. Discussion with G. Chen at JLAB turned out to be very helpful for ANSYS simulation. We also thank C. Ginsburg for the editorial help.

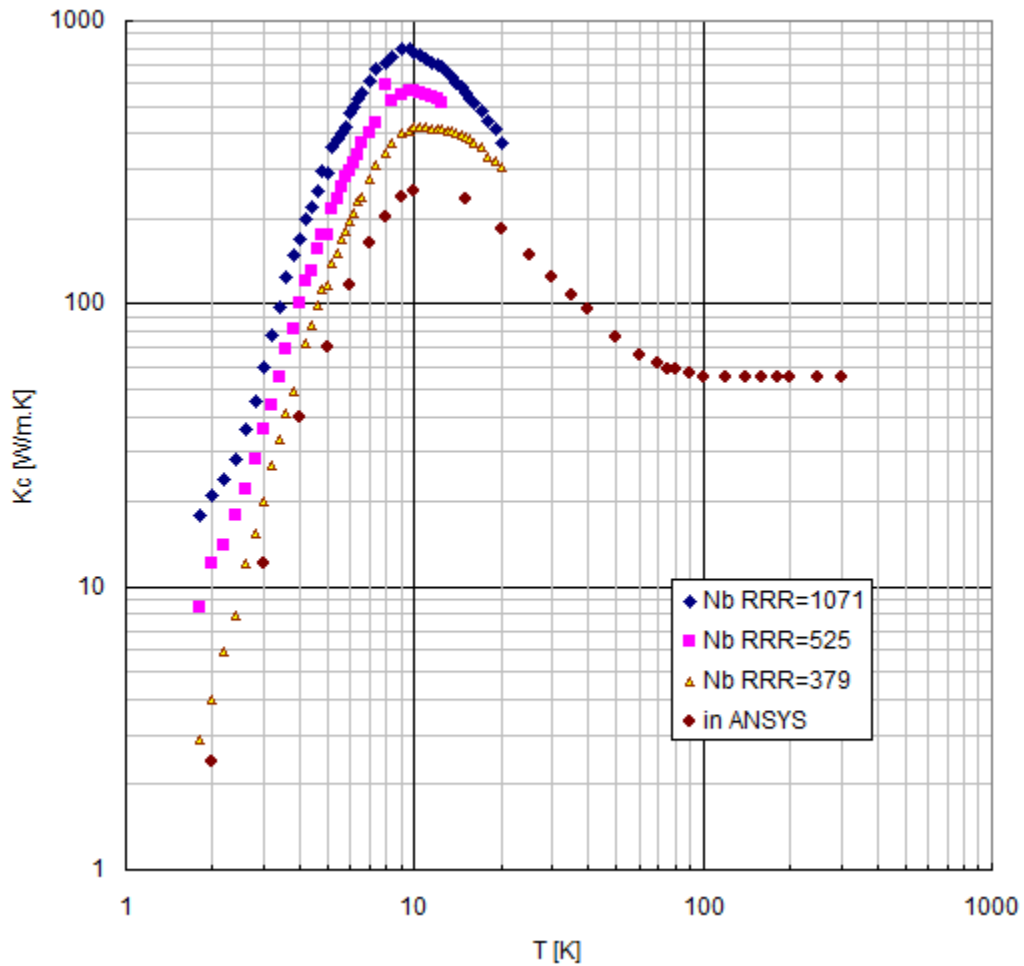
5. Appendix: Material Properties



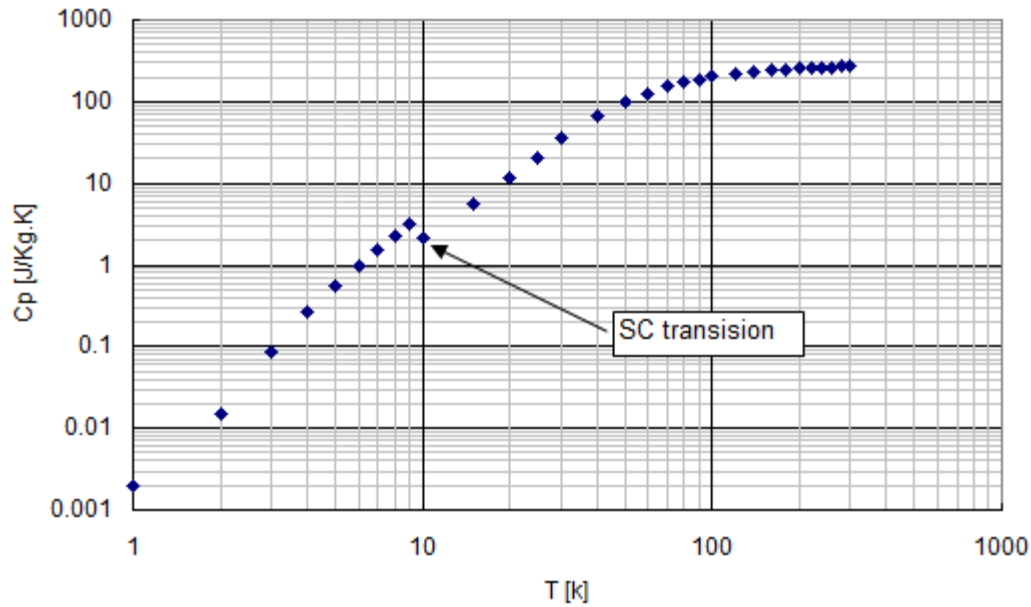
Appendix Figure 1: Sapphire thermal conductivity



Appendix Figure 2: Sapphire heat capacitance



Appendix Figure 3: Niobium thermal conductivity



Appendix Figure 4: Niobium heat capacitance

References

1. T. Khabiboulline et al., 3.9 GHz Superconducting Accelerating 9-Cell Cavity Vertical Test Results, Proc. of PAC2007, Albuquerque, New Mexico, USA (2007).
2. C.E. Reece et al., Thermal Conductivity Cryogenic RF Feedthroughs for Higher Order Mode Couplers, Proc. of PAC 2005, Knoxville, Tennessee, USA (2005).
3. P. Kneisel et al., Testing of HOM Coupler Designs on a Single Cell Niobium Cavity, Proc. of PAC 2005, Knoxville, Tennessee, USA (2005).
4. C.E. Reece et al., Diagnosis, Analysis, and Resolution of Thermal Stability Issues with HOM Couplers on Prototype CEBAF SRF Cavities, Proc. of SRF 2007, Peking University, Beijing, China (2005).
5. G. Wu et al., Electromagnetic Simulations of Coaxial HOM Coupler, Proc. of SRF 2005, Ithaca, New York, USA (2005).
6. W. Singer, Proceedings of SRF Materials Workshop, Fermilab, 2007.